Monthly Notices of the ROYAL ASTRONOMICAL SOCIETY

MNRAS **499,** 2744–2759 (2020) doi:10.1093/mnras/staa2936
Advance Access publication 2020 September 29

ATLASGAL – relationship between dense star-forming clumps and interstellar masers

S. J. Billington [1]★ J. S. Urquhart [1] C. König,[2] H. Beuther,[3] S. L. Breen [4] K. M. Menten,[2] J. Campbell-White [5] S. P. Ellingsen [6] M. A. Thompson,[7] T. J. T. Moore,[8] D. J. Eden [8] W.-J. Kim[9] and S. Leurini[2,10]

[1]*Centre for Astrophysics and Planetary Science, University of Kent, Canterbury CT2 7NH, UK*
[2]*Max-Planck-Institut für Radioastronomie, Auf dem Higel 69, D-53121 Bonn, Germany*
[3]*Max Planck Institute for Astronomy, Königstuhl 17, D-69117 Heidelberg, Germany*
[4]*SKA Organisation, Jodrell Bank Observatory, Macclesfield SK11 9DL, UK*
[5]*SUPA, School of Science and Engineering, University of Dundee, Nethergate, Dundee DD1 4HN, UK*
[6]*School of Mathematics and Physics, University of Tasmania, Private Bag 37, Hobart, Tasmania 7001, Australia*
[7]*Science and Technology Research Institute, University of Hertfordshire, College Lane, Hatfield AL10 9AB, UK*
[8]*Astrophysics Research Institute, Liverpool John Moores University, Liverpool Science Park, 146 Brownlow Hill, Liverpool L3 5RF, UK*
[9]*Instituto de Radioastronomía Milimétrica (IRAM), E-18012 Granda, Spain*
[10]*INAF-Osservatorio Astronomico di Cagliari, Via della Scienza 5, I-09047 Selargius (CA), Italy*

Accepted 2020 September 18. Received 2020 September 17; in original form 2019 December 11

ABSTRACT

We have used catalogues from several Galactic plane surveys and dedicated observations to investigate the relationship between various maser species and Galactic star-forming clumps, as identified by the APEX Telescope Large Area Survey of the Galaxy (ATLASGAL) survey. The maser transitions of interest are the 6.7 and 12.2-GHz methanol masers, 22.2-GHz water masers, and the masers emitting in the four ground-state hyperfine structure transitions of hydroxyl. We find clump association rates for the water, hydroxyl and methanol masers to be 56, 39, and 82 per cent, respectively, within the Galactic longitude range of $60^\circ > \ell > -60^\circ$. We investigate the differences in physical parameters between maser associated clumps and the full ATLASGAL sample, and find that clumps coincident with maser emission are more compact with increased densities and luminosities. However, we find the physical conditions within the clumps are similar for the different maser species. A volume density threshold of $n(\mathrm{H_2}) > 10^{4.1}$ cm^{-3} for the 6.7-GHz methanol maser found in our previous study is shown to be consistent across for all maser species investigated. We find limits that are required for the production of maser emission to be 500 $\mathrm{L_\odot}$ and 6 $\mathrm{M_\odot}$, respectively. The evolutionary phase of maser associated clumps is investigated using the *L*/*M* ratio of clumps coincident with maser emission, and these have similar *L*/*M* ranges ($\sim 10^{0.2}-10^{2.7}$ $\mathrm{L_\odot/M_\odot}$) regardless of the associated transitions. This implies that the conditions required for the production of maser emission only occur during a relatively narrow period during a star's evolution. Lower limits of the statistical lifetimes for each maser species are derived, ranging from $\sim 0.4-2 \times 10^4$ yr and are in good agreement with the 'straw man' evolutionary model previously presented.

Key words: Stars: formation – Stars: massive – ISM: molecules – submillimetre: ISM.

1 INTRODUCTION

Masers exist across the Galaxy and the different species of masers have been shown to trace certain physical processes and are associated with particular celestial objects (e.g. late-type stars, H II regions, star-forming regions; Elitzur 1992). Over the last decade, research has been devoted to the study of maser emission, where large-scale surveys have resulted in the production of large, comprehensive, and statistically representative catalogues of the various maser species (e.g. Caswell et al. 2010; Walsh et al. 2014; Qiao et al. 2016, 2018; Beuther et al. 2019). Catalogues of maser species have driven detailed investigations and theoretical studies into the environments and conditions required for their production (Sobolev, Cragg & Godfrey 1997; Norris et al. 1998; Cragg et al. 2001; Breen et al. 2010; Urquhart et al. 2013). Masers have been shown to be good chemical probes of star-forming environments (Menten 1997) and different species have been regularly shown to be coincident with each other in positional space (Forster & Caswell 1989; Menten et al. 1992; Menten 1997).

The Class II 6.7- and 12.2-GHz methanol (CH_3OH) masers, first reported by Menten (1991) and Batrla et al. (1987), respectively, have been found to be exclusively associated with intermediate- and high-mass young stellar objects (YSO; Minier et al. 2003; Xu et al. 2008; Breen et al. 2013; Urquhart et al. 2015; Billington et al. 2019). Therefore, the 6.7- and 12.2-GHz methanol masers provide a simple and convenient method for identifying potential regions of massive star formation. A number of observations have been made towards

★ E-mail: sjbb_astro@mail.com

these maser species and in-depth studies have been conducted (e.g. Menten et al. 1992; Phillips et al. 1998; Szymczak et al. 2002; Błaszkiewicz & Kus 2004; Goedhart, Gaylard & Van Der Walt 2005; Green et al. 2009). It is thought that the Class II methanol masers are produced in the accretion discs around young massive stellar objects (Norris et al. 1998), and are radiatively pumped in small, confined regions with temperatures of ∼150 K, methanol column densities of $>10^{15}$ cm^{-2} and volume densities of $>10^{8}$ cm^{-3} (Sobolev et al. 1997; Cragg et al. 2001). However, other studies have proposed different scenarios, such as the existence of these maser species within expanding shock waves or protostellar outflows (Walsh et al. 1998). Although, it could in fact be true that methanol masers exist in all of these situations (Minier 2000).

There also exist other maser species that are known to be associated with regions of star formation, such as the 22.2-GHz maser emission produced by water (H_2O; Cheung et al. 1969), and the four ground-state transitions of hydroxyl (OH; Weinreb et al. 1963) at 1612, 1665, 1667, and 1720-MHz. Observations of water masers indicate that these are found in outflows as well as circumstellar discs of both low- and high-mass YSOs (Claussen et al. 1996; Codella et al. 2004; Titmarsh et al. 2014, 2016), and are associated with regions of ongoing star formation. Elitzur, Hollenbach & Mckee (1989) presented a model for H_2O masers in star-forming regions, where masers are produced in post-shocked gas with initial densities of $n \sim 10^{7}$ cm^{-3} and temperatures of ∼400 K. Hydroxyl masers are known to trace a number of different environments. The most abundant transition at 1612-MHz is typically found in the expanding shells of evolved stars (Wilson & Barrett 1968; Elitzur, Goldreich & Scoville 1976), while the emission lines of 1665 and 1667-MHz have generally been found towards regions of star formation (Argon, Reid & Menten 2000; Qiao et al. 2014; Qiao et al. 2016). The 1720-MHz is the least frequently found and is generally observed towards shock excited regions within star formation sites and supernovae remnants (Claussen et al. 1999; Caswell 2004). However, none of these associations is exclusive and all four transitions can be found within different environments and even toward the same region (Caswell, Green & Phillips 2013; Walsh et al. 2016; Beuther et al. 2019). Cragg, Sobolev & Godfrey (2002) produced models of the OH masers, and found that OH masers require temperatures of ∼100 K, moderately high densities of $n = 10^{5}-10^{8}$ cm^{-3}, conditions which are likely to be met in all regions where OH masers are found.

As these three maser species are capable of tracing different physical conditions and processes, studies have been undertaken to investigate the relationship between the masers and environments where high-mass stars are born (e.g. Beuther et al. 2002; Breen et al. 2010; Breen & Ellingsen 2011; Urquhart et al. 2013, 2015). Studies have also investigated the relationship between different maser species (e.g. Forster & Caswell 1989; Menten 1997; Szymczak, Pillai & Menten 2005; Jones et al. 2020), and it has been shown that different maser transitions are often spatially associated with one another (within 15 arcsec). Ellingsen et al. (2007) presented a 'straw man' model for the evolution and relative time-scales of different maser species (water, methanol, hydroxyl) within regions of star formation. This model was further refined by Breen et al. (2010), who estimated relative lifetimes for each of the maser species. The sequence of events as described by this model state that during star formation, Class I (collisionally pumped) methanol masers occur first, followed by the appearance of water masers, produced in the post-shocked gas due to outflows associated with these object. Class II (radiatively pumped) masers are then produced in accretion discs due to the thermal output of the natal star. Finally, hydroxyl masers are seen towards developing H II regions, and as these H II regions evolve, they disrupt and disperse their environments, destroying the conditions necessary for any type of maser emission to exist (as indicated by the decreased detection rate of all maser types in the late evolutionary phases).

In three previous papers (Urquhart et al. 2013, 2015; Billington et al. 2019), we have presented a detailed analysis of the 6.7-GHz methanol masers, as identified by the Methanol MultiBeam survey (MMB; Green et al. 2009), and submillimetre dust emission, as identified by the APEX Telescope Large Area Survey of the Galaxy (ATLASGAL; Schuller et al. 2009). These works identified the almost ubiquitous association between the 6.7-GHz maser and dust emission (∼99 per cent), and showed that this maser species has a well-defined turn-on and termination point, existing for a distinct amount of time in the evolutionary time-scale of massive star formation, with a statistical lifetimes of 3.3×10^{4} yr (Billington et al. 2019). The findings of this study support the theoretically derived value (Van Der Walt 2005; $2.5-4.5 \times 10^{4}$ yr). Given the availability of large-scale water and hydroxyl surveys, it is possible to extend our previous work and fully test the 'straw man' model presented by Ellingsen et al. (2007) and Breen et al. (2010) by investigating the lifetimes and evolutionary time-scales of multiple maser species.

This study will extend the work of Billington et al. (2019) by investigating the physical properties of dense Galactic clumps associated with each maser transition, for which catalogues have been produced from a number of Galactic surveys. The Galactic surveys of interest are: the MMB survey (Caswell et al. 2010, 2011; Green et al. 2010, 2012; Breen et al. 2015), The H I/OH/Recombination line survey (THOR; Beuther et al. 2016, 2019), the Southern Parkes Large-Area Survey in Hydroxyl (SPLASH; Dawson et al. 2014; Qiao et al. 2014, 2016), the H_2O southern Galactic Plane Survey (HOPS; Walsh et al. 2011, 2014) and observations of 12.2-GHz methanol masers undertaken by Breen et al. (2012a, 2012b, 2014, 2016). These surveys are described in Section 2. Along with investigating the physical properties of maser associated clumps, we derive statistical lifetimes for each of the masers species and identify their positions in the evolutionary time-scales of star formation.

The structure of this paper is as follows: In Section 2, we describe the archival survey data that will be used throughout the study. In Section 3, we describe the matching procedure used for the maser species of interest. Section 4 presents the derivation of the various physical parameters of maser associated dust clumps, along with the corresponding uncertainties. In Section 5, we discuss various aspects of the different maser samples, along with presenting the statistical lifetimes for each maser species. A summary of our findings is given in Section 6.

2 SURVEY DESCRIPTIONS

Fig. 1 shows the survey coverages for each of the surveys that are utilized in this study. In Table 1, we present a summary of the coverages for each survey.

2.1 Descriptions of maser surveys

2.1.1 The HOPS

The HOPS (Walsh et al. 2011) is an unbiased survey of 100 deg^2 of the Galactic plane ($30^\circ \geq \ell \geq 290^\circ$, $|b| < 0.5^\circ$). HOPS was performed using the Australia Telescope National Facility (ATNF) Mopra 22-m radio telescope and detected 540 sites of 22.2-GHz H_2O maser emission (Walsh et al. 2011). Walsh et al. (2014) performed follow-up observations of these maser sites using the

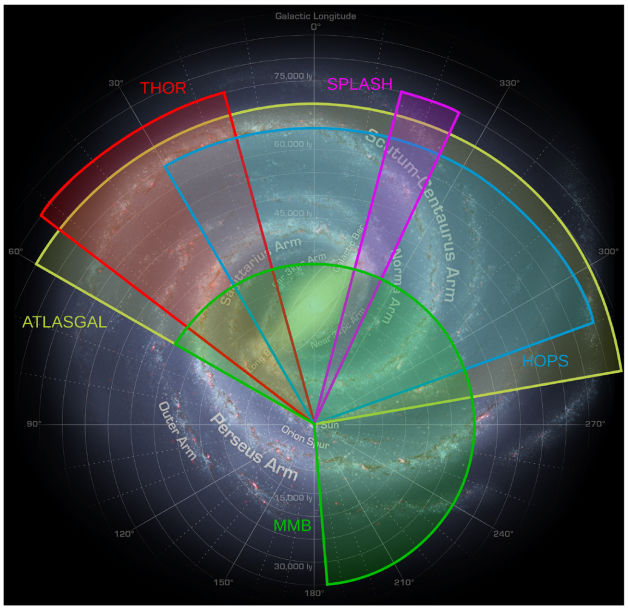

Figure 1. Image depicting the Galactic longitude coverages for the Galactic plane surveys that are utilized in this study (courtesy of NASA/JPL-Caltech/R. Hurt (SSC/Caltech). The approximate coverage of each survey is shown along with each surveys' corresponding name. The length of each sector is arbitrary.

Table 1. Galactic Longitude coverages for each survey presented in this study.

Survey name	Maser species	Sensitivity (mJy)	Survey coverage
HOPS	H_2O	15–167	$30^\circ \geq \ell \geq 290^\circ$
THOR	OH	∼10	$66\overset{\circ}{.}8 \geq \ell \geq 14\overset{\circ}{.}5$
SPLASH	OH	∼65	$344^\circ \geq \ell \geq 334^\circ$
MMB	Class II CH_3OH	∼170	$60^\circ \geq \ell \geq 186^\circ$
ATLASGAL	870-μm continuum	∼60	$60^\circ \geq \ell \geq 280^\circ$

Australia Telescope Compact Array (ATCA), to provide accurate positions for individual maser spots within 1 arcsec. The typical noise for these observations was 15–167 mJy. The higher resolution observations identified 631 maser sites (collections of maser spots) in the 540 regions detected by Mopra; these consisted of 2790 individual spectral features (maser spots).

Out of the 631 maser sites detected in Walsh et al. (2014), 433 were identified as being associated with star formation, 121 sites with evolved stars and the remaining 77 were classified as unknown. They also found that evolved stars tend to have more maser spots than those associated with star formation. Furthermore, they found that maser sites associated with evolved stars are much more clustered around localized positions than the full area of star formation regions. The linear positions of maser spots within star formation regions present features that are both parallel and perpendicular to known outflows, where H_2O masers are thought to originate.

2.1.2 THOR line survey

THOR (Beuther et al. 2016) line survey of the inner Milky Way has surveyed $14\overset{\circ}{.}5 \leq \ell \leq 66\overset{\circ}{.}8$ and $|b| < 1\overset{\circ}{.}25$ of the Galactic plane using the Karl Jansky Very Large Array in the C-array configuration. The THOR survey has observed a number of different spectral lines, including the H I 21 cm, 19 of the H$n\alpha$ radio recombination lines and the four ground-state transitions of the hydroxyl maser, as well as continuum emission between 1 and 2-GHz (Bihr et al. 2016; Wang et al. 2018). The survey has angular resolutions of ∼12.5–19 arcsec, with a spectral resolution of 1.5 km s^{-1}, and typical rms noise levels of ∼10 mJy.

Recently, THOR has produced an unbiased catalogue of the four OH maser emission lines at 1612, 1665, 1667, and 1720-MHz (Beuther et al. 2019). The catalogue is comprised of OH maser sources in the northern hemisphere, tracing a number of different astronomical phenomena, as previously described in Section 1. We do note here that within the THOR survey, the 1667-MHz maser was not covered in ∼50 per cent of the survey (below $\ell = 29\overset{\circ}{.}2$, between $31\overset{\circ}{.}5$ and $37\overset{\circ}{.}9$ and between $47\overset{\circ}{.}1$ and $51\overset{\circ}{.}2$), however, this will not affect the results and statistics presented in this study.

2.1.3 The SPLASH

The SPLASH is an unbiased southern Galactic plane survey of the four ground-states transitions of the hydroxyl molecule, undertaken using the Parkes 64-m telescope and utilizing the H–OH receiver. The first results of this survey are presented in Dawson et al. (2014) and covers the Galactic plane between longitudes 334° and 344° and latitudes $|b| < 2^\circ$. Within this region, the SPLASH survey has detected a total of 495 masers, across the four ground transitions of hydroxyl.

Qiao et al. (2016) presented accurate positions of the masers identified within the pilot region. These observations were undertaken using the ATCA, with angular resolutions of between 4 and 13 arcsec, spectral resolution of 0.09 km s^{-1} and typical rms noise levels of ∼65 mJy. The catalogue presented in Qiao et al. (2016) provides a further sample of hydroxyl masers in the southern Galactic plane and we use these to supplement the THOR survey maser catalogue.

2.1.4 Class II Methanol masers (6.7 and 12.2 GHz)

The MMB (Green et al. 2009) survey has surveyed the Galactic plane between $60^\circ \geq \ell \geq 186^\circ$ and $|b| < 2^\circ$, and has produced a catalogue of 972 emission sites of the Class II 6.7-GHz methanol maser across the Galaxy (Caswell et al. 2010, 2011; Green et al. 2010, 2012; Breen et al. 2015). Initial detections were made using the ATNF Parkes 64-m radio telescope, and were followed up with ATCA or the Multi-Element Radio Linked Interferometer Network (MERLIN; Thomasson 1986) to determine accurate positions (<1 arcsec) to maser emission sites if those positions were not available in the literature. The average noise in survey cubes was 170 mJy. It is likely that the MMB survey accounts for the majority of 6.7-GHz methanol masers across the Galaxy, as it has been shown that away from the Galactic plane, 6.7-GHz maser emission is rare (Yang et al. 2017, 2019). This is also consistent with them being only associated with high-mass star formation.

Breen et al. (2012a, 2012b, 2014, 2016) have produced a number of MMB follow-up observations towards sites of 6.7-GHz methanol masers, searching for the class II 12.2-GHz methanol maser transition. The 12.2-GHz maser is the strongest and most widespread class II methanol maser line after the 6.7-GHz transition, and over the same coverage as the MMB survey ($60^\circ \geq \ell \geq 186^\circ$), Breen et al. detected 432 12.2-GHz masers. Breen et al. (2012a, b, 2014, 2016) also concluded that the 12.2-GHz maser occurs within star formation regions at a slightly later stage of evolution than regions that are only associated with the 6.7-GHz transition. This was explained due to the 12.2-GHz methanol masers being associated with 6.7-GHz masers that have relatively higher flux densities and peak luminosities.

Furthermore, 12.2-GHz methanol masers are also more likely to be found towards 6.7-GHz methanol masers with associated OH masers (Breen et al. 2010). The estimated lifetime of the 12.2-GHz masers is estimated to be in the range 1.5×10^4 and 2.7×10^4 yr (Breen et al. 2010).

It is worth noting that as the 12.2-GHz maser observations are targeted towards known positions of 6.7-GHz masers, this sample may not be regarded as an independent sample. However, no previous studies have resulted in the serendipitous detections of 12.2-GHz methanol masers, and all currently known 12.2-GHz masers have been found with a 6.7-GHz counterpart. Also, previous searches (Caswell et al. 1995; Błaszkiewicz & Kus 2004) have shown that 12.2-GHz methanol maser emission is rarely brighter than any associated 6.7-GHz methanol maser emission. Therefore, it is not unreasonable to assume that the observations conducted by Breen et al. (2012a, 2012b, 2014, 2016) account for the majority of the 12.2-GHz methanol masers within the MMB survey coverage ($60^\circ \geq \ell \geq 186^\circ$).

2.2 ATLASGAL survey

ATLASGAL (Schuller et al. 2009) has mapped dust emission at 870-μm across 420 deg^2 of the Galactic plane, between Galactic longitudes $60^\circ \geq \ell \geq 280^\circ$ and latitudes $|b| < 1.5^\circ$. ATLASGAL is the largest and most sensitive ground-based submillimetre survey to date and has produced a catalogue of over 10 000 dense clumps within the Galaxy (Contreras et al. 2013; Csengeri et al. 2014; Urquhart et al. 2014b). The Large APEX Bolometer Camera (LABOCA; Siringo et al. 2009) was used to conduct the survey. The APEX telescope has a dish size of 12 m allowing for a full width at half-maximum (FWHM) resolution of 19.2 arcsec at this wavelength.

Urquhart et al. (2018) produced a catalogue of physical parameters for a large fraction of the ATLASGAL compact source catalogue (∼8 000), outside of the Galactic centre region ($5^\circ < |\ell| < 60^\circ$ and $|b| < 5^\circ$). The Galactic centre region was omitted from this study to reduce source confusion and difficulty in determining reliable kinematic distances. This catalogue includes representative samples of all of the earliest stages of massive star formation. Following the procedures first established for a representative sample of ∼100 ATLASGAL sources (König et al. 2017), emission maps from the HiGAL survey (Molinari et al. 2010) were used to fit the spectral energy distributions (SEDs) in order to derive dust temperatures and bolometric luminosities of embedded objects. Follow-up molecular line observations of the ATLASGAL emission maps (e.g. CO, NH_3, N_2H^+; see table 1 of Urquhart et al. 2018 for a complete list of observations) have determined radial velocities which, along with the Galactic rotation curve, have been used to derive distances to ∼8 000 regions (∼79 per cent of the full ATLASGAL sample). These distances have been used to determine the properties of dense clumps across the Galaxy as presented in Urquhart et al. (2018). Every ATLASGAL source has been classified into one of four evolutionary groups based on infrared or radio counterparts and are defined as quiescent, protostellar, YSO, and H II region (König et al. 2017).

3 MASER ASSOCIATIONS

This study will only focus on the Galactic coverage between $5^\circ < |\ell| < 60^\circ$ and $|b| < 1.5^\circ$, the same coverage as Urquhart et al. (2018), to ensure we have accurate determinations for the physical properties of clumps associated with any maser transition.

By using the catalogues of the surveys mentioned in the previous section, we have attempted to associate multiple maser transitions to dense clumps as found in the ATLASGAL survey. These maser transitions are the 6.7-GHz and 12.2-GHz methanol maser, 22.2-GHz water maser and the four hydroxyl maser emission lines at 1612, 1665, 1667, and 1720-MHz. We have utilized the 6.7-GHz methanol maser matches with the ATLASGAL survey reported in Urquhart et al. (2013) and Billington et al. (2019) but have not included clumps identified from the JCMT Plane Survey (JPS; Moore et al. 2015; Eden et al. 2017; Billington et al. 2019) as the data from JPS will provide no further information for this study. We have also chosen not to utilize the targetted observations towards sites of 6.7-GHz methanol maser emission presented in Urquhart et al. (2015) that were beyond the boundaries of the ATLASGAL survey.

When referring to a specific maser species or transition in this study, the corresponding frequency of that maser will always be given, in contrast, the term 'maser' used independently will refer to all the maser transitions.

3.1 Spatial matching

Initial matches were identified using a 90 arcsec search radius between maser emission and the 870-μm peak dust emission. This radius is the 3σ value of the effective radius distribution for ATLASGAL sources and so 99.7 per cent of dust continuum sources have a radius of less than this size. Images have been created from the ATLASGAL 870-μm emission maps, so that each match could be confirmed visually. A match was confirmed if the maser source was within the 3σ boundary of the 870-μm emission and all masers found beyond this boundary have been removed from any further analysis, as these are unlikely to be associated with star formation. We find 549 OH (429 from THOR and 120 from SPLASH), 359 water and 392 12.2-GHz masers sites that are spatially coincident with dust emission (within 3σ). A cumulative distribution function of the angular offsets for each of the maser species can be found in the upper panel of Fig. 2. It can be seen from this figure that the majority of masers (∼90 per cent) lie within 10 arcsec of a dust continuum peak. As the majority of star formation is concentrated towards the highest column density regions in the centre of clumps (Urquhart et al. 2014a), this provides further confirmation that the masers are associated with star formation. It can also be seen from the upper panel in Fig. 2 that there are no significant differences in the spatial offsets between the various maser species. However, they may be differences on scales less than 10 arcsec but the resolution of the data is not sufficient to investigate this.

3.2 Velocity offsets

Molecular line velocities of the dense clumps are available for the majority of masers and for a large portion of the ATLASGAL survey (see table 1 of Urquhart et al. 2018 for a complete list of observations and references). We use these measurements to examine the correlation between the masers and the dense clumps to confirm their associations. The difference between maser median velocity and clump median velocity has been calculated for all of the maser species that are spatially coincident. The cumulative distribution functions of these distributions can be found in the lower panel of Fig. 2. It can be seen from this Figure that water masers appear to have larger velocity offsets, which is consistent with this type of maser being associated with protostellar outflows.

In Fig. 3, we show the velocity offsets for the different maser species and these have been fitted with Gaussian profiles. The Gaussian fits appear to be a reasonable model for all of the velocity distributions. To confirm our maser associated sample, we have opted to only include clumps with a maser source that has a median velocity

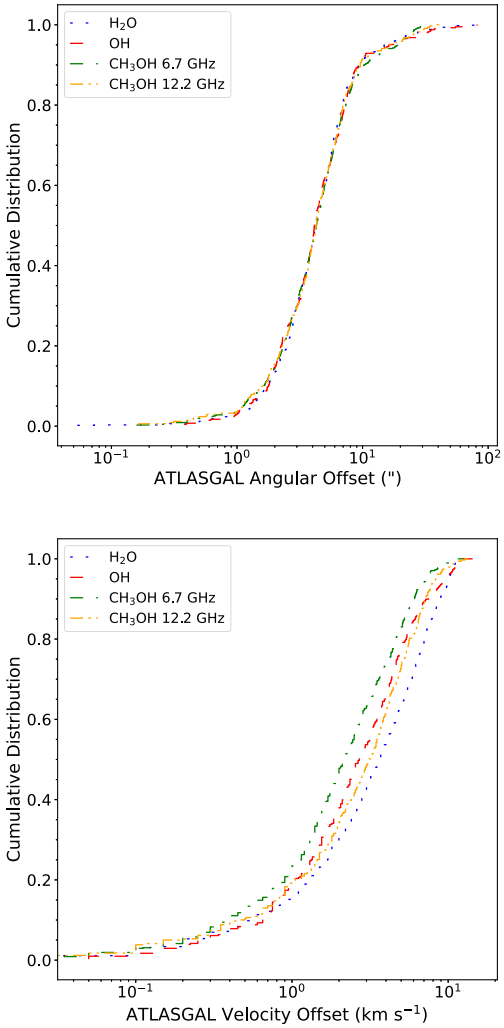

Figure 2. Cumulative distribution functions of the maser-ATLASGAL angular and velocity offsets in the upper and lower panels respectively. Each coloured line represents a different maser species as shown by the legend in the top left-hand corner of each plot. Both panels present the same maser associated clump sample, i.e. those that are within the spatial and velocity matching criteria as explained in the text.

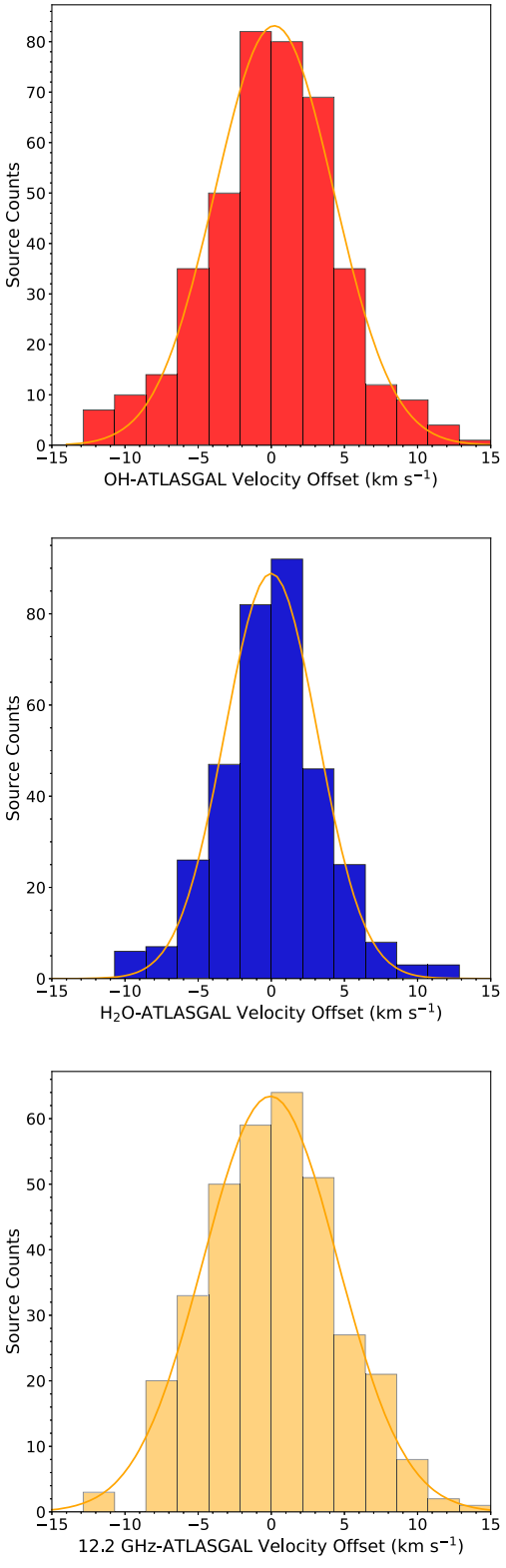

Figure 3. Histograms presenting the velocity offsets between the median maser velocities and the ATLASGAL molecular line velocities. The panels present the hydroxyl, water, and 12.2-GHz methanol maser velocity distributions in the upper, middle, and lower panels, respectively. The distributions have been truncated at −15 and 15 km s^{-1}. A Gaussian profile has been fitted to each histogram and is shown as the solid yellow lines in each panel.

difference of less than 3σ, which is calculated from the Gaussian models. This likely accounts for any possible line-of-sight alignments between masers and clumps that may not be spatially coincident. It is likely that masers with a high-velocity difference compared to a spatially aligned clump, may in fact not be associated with each other. Since the focus of this study is on the dense clumps associated with maser emission and not the masers themselves, this will help to refine the true sample of maser associated clumps. The 3σ values for the different distributions are 11.56, 11.92, and 13.89 km s^{-1} for the H_2O, OH, and 12.2-GHz methanol masers, respectively. The 3σ value for the 6.7-GHz methanol masers is taken from Billington et al. (2019) as 13.5 km s^{-1}.

3.3 Total matched sample

We have matched a number of different maser species to dense clumps across the Galaxy as identified by the ATLASGAL survey. Our sample has been constrained using the positional and velocity

Table 2. Total matches for each maser species and the ATLASGAL catalogue between Galactic longitudes $60^\circ > \ell > -60^\circ$, where all matches are below our 3σ threshold in both positional and velocity space. The percentage of associated dust clumps within each survey coverage is also given. Errors have been calculated using Binomial statistics.

Maser transition	Maser–dust associations	Percentage of associated dust clumps[a]
CH_3OH 6.7-GHz	839/918 (91 ± 0.9%)	8.5%
CH_3OH 12.2-GHz	340/414 (82 ± 1.9%)	3.2%
H_2O 22.2-GHz	345/614 (56 ± 1.4%)	2.0%
OH 1612-MHz	43/1378 (3 ± 0.5%)	0.9%
OH 1665-MHz	238/394 (60 ± 2.5%)	3.6%
OH 1667-MHz	96/226 (42 ± 3.2%)	1.2%
OH 1720-MHz	31/63 (49 ± 6.3%)	0.7%

[a]Number of ATLASGAL sources with an associated detected maser.

offsets as previously described. The number of maser associations for each maser transition can be found in Table 2.

We find that there is no difference in the spatial offsets between each maser species and their associated dust clump. The average offset between any maser species and the peak dust emission is ∼6 arcsec with the 90 per cent range of the maser samples having offsets between 1.7 and 10.3 arcsec. The absolute velocity differences for all of the maser species range between 2.8–4.3 km s^{-1} with the 6.7-GHz methanol maser having the smallest average velocity offset of 2.8 km s^{-1}.

Out of the 807 hydroxyl maser sites identified by the THOR survey, we have matched 294 to 141 individual dense clumps identified by the ATLASGAL survey. This is an association rate of 36 per cent with 2.1 maser sources per clump on average. The majority of clumps contain more than two maser sources (75/141), and the remaining 66 sources are only associated with a single maser. Of the 75 clumps with multiple maser associations, there exist four clumps with five maser sources and also another four which contain more than five maser sources. As the average number of masers per clumps is 2.1, we find that only three of these eight sources have a significantly[1] large number of masers (G030.703–00.067 and G031.412+00.307 with nine and G030.823–00.156 with eight; these three regions are associated with the W43 star-forming complex; Motte, Schilke & Lis 2002). For the 495 OH maser sites identified by the SPLASH survey, we have matched 114 of these to 24 individual ATLASGAL sources, giving an average number of maser per clump of five and association rate of 23 per cent. Five clumps have a significant number of masers (G338.876–00.084 with 8, G339.986–00.426 with 10, G340.054–00.244 with 12, G340.784–00.097 with 13 and G344.227–00.569 with 8), with the maximum number of masers being 13, associated with G340.784–00.097.

As both surveys cover all four hydroxyl emission lines, we find the 1612, 1665, 1667, and 1720-MHz transitions to have corresponding association rates with 165 dust clumps of 3, 60, 42, and 51 per cent, respectively. Fig. 4 presents a Venn diagram of the matches between clumps and the four different hydroxyl transition lines. We find that 145 of the 165 dust continuum sources are associated with a 1665-MHz maser, with only 26 dense clumps containing a 1720-MHz maser, showing that the 1665-MHz are more commonly found towards regions of star formation. The mean association rates for 1665, 1667, and 1720-MHz are all roughly 50 per cent, however, the 1612-MHz has an association rate of 3 per cent. The lower number of associated 1612-MHz masers is expected due to this maser transition being larger associated with the expanding shells of AGB stars. Furthermore, we find the majority of hydroxyl masers that are associated with a clump (96 per cent) to be associated with either a YSO or H II region as identified by the ATLASGAL survey. We only find eight clumps that are coincident with a hydroxyl maser (1665 or 1667-MHz) and that are associated with a protostellar object (identified by a weak mid-infrared counterpart in the ATLASGAL survey).

[1]Significance is based on the 3σ value calculated using Poisson statistics.

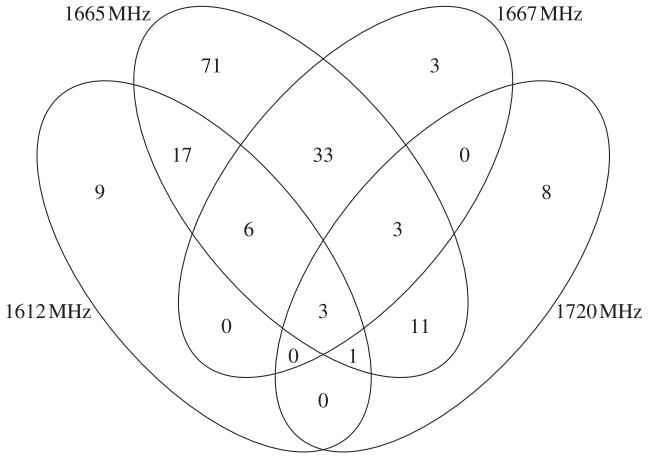

Figure 4. A Venn diagram presenting the number of ATLASGAL sources associated with the different transition lines of the hydroxyl maser.

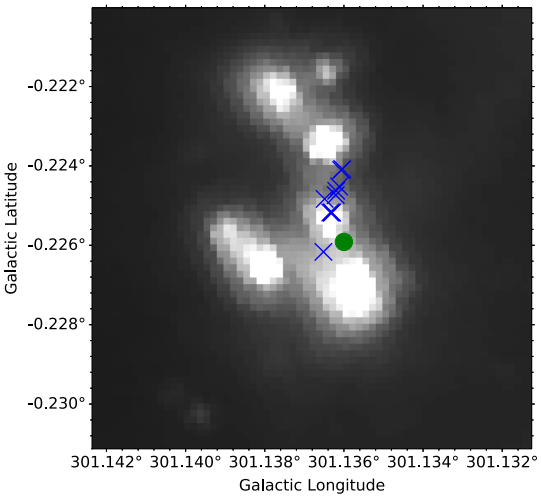

Figure 5. An example GLIMPSE 8-μm image of the region G301.136–00.226. The positions of water masers associated with this region have been overplotted as blue crosses and the associated 6.7-GHz methanol masers as green filled circles. It is likely that these masers are associated with a known protostellar outflow in the region (see the text for details).

We have matched 345 water maser sites (978 maser spots), presented in Walsh et al. (2014), to 291 dust continuum sources, an association rate of 55 per cent with a mean maser number of spots per clump of 1.2, which is lower than the overall rate found for the hydroxyl masers. We find that out of the 291 matched dust continuum sources, there is one source with 10 maser spots (G301.136–00.226), a significant number of maser spots, which is also associated with a 6.7-GHz methanol maser. An 8-μm infrared GLIMPSE legacy survey (Churchwell et al. 2009) image of this region is presented in Fig. 5. A linear alignment between the water masers can be seen, likely due to an outflow originating in the region (Henning et al. 2000; Guzmán

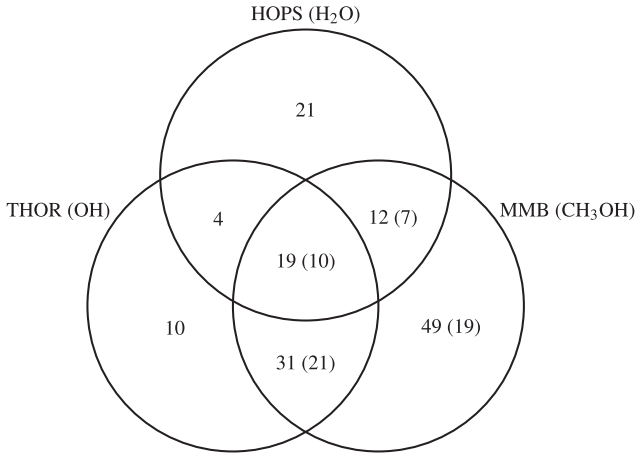

Figure 6. A Venn diagram presenting the number of ATLASGAL sources and the corresponding associated masers between Galactic longitudes, 14.°5 $< \ell <$ 30°, and Galactic latitudes, $|b| < 0.5°$. The values in brackets are the values for the 12.2-GHz methanol masers, all of which are associated with a 6.7-GHz maser counterpart.

et al. 2012). This is consistent with the idea that the morphology of water masers trace outflows (e.g. Claussen et al. 1996).

For the 432 emission sites of the 12.2-GHz, as identified by Breen et al. (2012a, 2012b, 2014, 2016), we find that 340 are associated with 330 ATLASGAL sources. The majority of clumps (320; 96 per cent) that are associated with a 12.2-GHz methanol maser only host a single maser, with the remaining clumps (10; 3 per cent) hosting two masers. No clumps are associated with more than two 12.2-GHz methanol masers. Matching statistics for the 6.7-GHz methanol masers are taken unchanged from Billington et al. (2019). This study produced a sample of 839 6.7-GHz methanol masers (identified by the MMB survey) that are associated with dust continuum emission, also with an average of 1 maser site per clump. The percentage of the number of dust clumps associated with each maser species can be found in Table 2.

3.4 Common Spatial Area

Each of the surveys presented in this study has differing Galactic coverages and while this has no impact on the fractional associations between individual masers species and the dust emission, to be able to compare associations rates for different sources, we need to investigate a common region. Fortunately, due to the coverages of the presented surveys, there exist two windows on the Galactic plane where all four maser species were observed in at least one survey. The first window is positioned between Galactic longitudes of 14.°5$< \ell <$ 30° and Galactic latitudes of $|b| < 0.5°$, and the second is between Galactic longitudes of $334° < \ell < 335°$ and Galactic latitudes of $|b| <$ 0.5°(see Fig. 1). Due to the superior sensitivity of the THOR survey, we have chosen to use this first common spatial area to investigate the relationships between the maser species themselves and how they relate to the dust continuum.

Within this window, we find that there are 1 263 ATLASGAL sources, however, only 146 (12 per cent) of these are associated with maser emission. This low association rate may suggest that masers are not always present within clumps or they may only be associated with a particular stage of star formation. The matches between this subsample of clumps and the various maser transitions are shown in Fig. 6 in the form of a Venn diagram. As all of the 12.2-GHz masers will have a 6.7-GHz counterpart, due to the nature of the observations, they are included in brackets with the 6.7-GHz matching values. We find that within this overlapping coverage window there are 64, 56, 57, and 111 clumps associated with hydroxyl (at least one transition), water, 12.2-GHz methanol and 6.7-GHz methanol masers, respectively.

Out of the 146 maser associated clumps in this window, 47 ± 4 per cent of them are associated with multiple maser species. We find that 76 ± 4 per cent of the clumps are associated with a 6.7-GHz methanol maser, significantly higher than the number of clumps associated with water (38 ± 4 per cent) and hydroxyl masers (44 ± 4 per cent). It can also be seen that 12.2-GHz methanol masers are present in 39 ± 4 per cent of clumps, showing that only approximately half of 6.7-GHz maser have a 12.2-GHz counterpart. This result was found in the 12.2-GHz maser follow-up catalogues (e.g. Breen et al. 2012a) but which differs from previous studies of this association rate, e.g. Błaszkiewicz & Kus (2004), who found a rate of 19 per cent. This is likely due to the improved sensitivity of the Breen et al. (2012a, 2012b, 2014, 2016) observations and the relative dimness of 12.2-GHz methanol masers compared to the 6.7-GHz methanol masers. The 6.7-GHz methanol maser also accounts for the majority of masers that are found in isolation at 58 ± 4 per cent, while the water and hydroxyl masers are only found in isolation (no association with other masers in the same clump) 25 ± 4 and 12 ± 4 per cent of the time, respectively.

It appears to be quite rare to find only a water maser and hydroxyl maser to be associated with the same source (only 4 out of 146 clumps), whereas the majority of these masers are always found with a methanol maser counterpart. Beuther et al. (2002) used a sample of 29 star-forming regions and found that ∼62 per cent of 6.7-GHz methanol masers are associated with water emission and that ∼65 per cent of water masers are associated with a 6.7-GHz methanol maser. Our results differ slightly in that we find only 28 ± 6 per cent 6.7-GHz methanol masers are associated with water emission, and 55 ± 7 per cent of water masers are associated with 6.7-GHz methanol emission. Breen et al. (2018) presented a comparison between the MMB and HOPS catalogues, and while they also found that 28 per cent of methanol masers have a water counterpart, they only found that 40 per cent of water masers are seen coincident with methanol masers (both 6.7 and 12.2-GHz). Although, this disparity is likely due to the matching parameters used in each study and their associated observing sensitivities. Furthermore, Titmarsh et al. (2014, 2016) conducted studies towards known positions of 324 6.7-GHz methanol masers and found that ∼46 per cent and ∼50 per cent of the 6.7-GHz methanol masers have a water emission counterpart, respectively. The differences in the association rates between the water and methanol masers is likely due to the differing sensitivities for each set of observations and the intrinsic variability of water masers (due to accretion and outflows associated within young stars and protostellar objects). However, the differences could also be due to the smaller sample sizes in previous studies.

4 PHYSICAL PARAMETER CALCULATIONS

In the following subsections, we describe how the physical parameters of our sample are derived and present the statistics for each in Table 3. The ATLASGAL catalogue provides an effective radius for each clump larger than the beam size of the survey; this radius is the intensity weighted flux density distribution (Contreras et al. 2013) scaled by a value of 2.4, which gives a reasonable approximation of the observed clump size (Rosolowsky et al. 2010). However, it was shown by Urquhart et al. (2018) that evolving clumps appeared to be associated with increasing radius, mass and

Table 3. Total statistical parameters for all maser associated clumps, determined within our matching criteria, within the Galactic longitude range $5^\circ < |\ell| < 60^\circ$. The values in brackets show the statistics from a distance-limited sample between 2 and 5 kpc.

Parameter	Number	Mean	Standard deviation	Standard error	Median	Minimum	Maximum
Distance (kpc)							
Maser sample	804 (273)	5.80 (3.07)	3.84 (0.48)	0.14 (0.03)	4.60 (3.10)	0.10 (2.10)	24.20 (3.90)
ATLASGAL	7743 (3014)	4.90 (3.10)	3.31 (0.46)	0.04 (0.01)	3.60 (3.10)	0.00 (2.10)	24.20 (3.90)
Radius (pc)							
Maser sample	768 (263)	0.35 (0.20)	0.27 (0.08)	0.01 (0.00)	0.26 (0.18)	0.01 (0.08)	1.85 (0.53)
ATLASGAL	5478 (2108)	0.41 (0.27)	0.31 (0.11)	0.00 (0.00)	0.32 (0.25)	0.00 (0.07)	2.89 (0.93)
Temperature (K)							
Maser sample	830 (258)	23.91 (23.78)	5.26 (5.66)	0.18 (0.35)	23.42 (23.16)	11.76 (12.13)	51.23 (51.23)
ATLASGAL	9928 (2952)	19.40 (18.93)	5.72 (5.89)	0.06 (0.11)	18.44 (17.76)	5.87 (7.89)	59.96 (51.23)
log[Luminosity ($L_\odot$)]							
Maser sample	780 (258)	3.99 (3.65)	1.00 (0.84)	0.04 (0.05)	4.00 (3.53)	− 0.22 (1.74)	6.91 (5.83)
ATLASGAL	7601 (2952)	2.95 (2.66)	1.03 (0.89)	0.01 (0.02)	2.89 (2.56)	− 0.28 (0.55)	6.91 (5.93)
log[Clump mass ($M_\odot$)]							
Maser sample	768 (256)	2.63 (2.30)	0.68 (0.41)	0.02 (0.03)	2.71 (2.32)	− 1.05 (1.23)	4.40 (3.28)
ATLASGAL	7460 (2909)	2.52 (2.32)	0.61 (0.34)	0.01 (0.01)	2.53 (2.33)	− 1.05 (1.03)	4.40 (3.43)
log[L/M ratio ($L_\odot/M_\odot$)]							
Maser sample	768 (256)	1.38 (1.36)	0.63 (0.65)	0.02 (0.04)	1.35 (1.30)	− 0.43 (−0.43)	3.25 (3.25)
ATLASGAL	7460 (2909)	0.44 (0.34)	0.89 (0.91)	0.01 (0.02)	0.42 (0.29)	− 2.40 (−2.40)	3.30 (3.30)
log[Volume density (cm^{-3})]							
Maser sample	744 (248)	4.86 (5.06)	0.54 (0.43)	0.02 (0.03)	4.83 (5.02)	3.40 (4.11)	6.90 (6.90)
ATLASGAL	5354 (2052)	4.59 (4.72)	0.48 (0.39)	0.01 (0.01)	4.56 (4.70)	2.95 (3.67)	6.90 (6.90)
log[Free-Fall Time (yr)]							
Maser sample	744 (248)	5.27 (5.17)	0.27 (0.22)	0.01 (0.01)	5.28 (5.19)	4.25 (4.25)	6.00 (5.64)
ATLASGAL	5354 (2052)	5.41 (5.34)	0.24 (0.20)	0.00 (0.00)	5.42 (5.35)	4.25 (4.25)	6.22 (5.86)

decreasing volume density measurements. They determined that this was due to an observational bias. As Galactic clumps evolve their average temperature increases, which in turn, results in the extended envelope of these regions becoming bright enough to be detected by the ATLASGAL survey. Therefore, the apparent size and mass of sources appeared to increase (and density decreasing proportionally) during evolution. Billington et al. (2019) eliminated this bias by only considering the flux from within the FWHM contour of each 870-μm source. It was shown that this technique effectively removed the observational bias (see fig. 8 of Billington et al. 2019).

Throughout this study, we also use a distance-limited sample, from 2 to 5 kpc, to reduce any distance-related biases that may exist within the sample.

4.1 FWHM radius, clump mass, and volume density

The FWHM radius and mass values used in this study are taken directly from Billington et al. (2019) and are scaled from the values found in Urquhart et al. (2018) by using the ratio between the FWHM flux and the total flux of each clump.

The FWHM volume densities have also been calculated using the FWHM radii and FWHM masses in the same way as described in Billington et al. (2019):

$$n\,(\mathrm{H_2}) = \frac{3}{4\pi}\frac{M_{\mathrm{fwhm}}}{\mu m_p R^3_{\mathrm{fwhm,pc}}}, \quad (1)$$

where $n(\mathrm{H_2})$ is the hydrogen number density of clumps, μ is the mean molecular weight of the gas (taken here to be 2.8), and m_p is the mean proton mass. M_{fwhm} and R_{fwhm} are the FWHM mass and FWHM radius, respectively. Here, the clumps are assumed to be spherical and not extended along the line of sight. Fig. 7 presents the distributions of the clump FWHM radius, FWHM mass, and FWHM volume density in the upper, middle, and lower panels respectively. It can be seen from the upper panels of this Figure that maser associated clumps are significantly more compact. Although as shown in the middle panels, the masses of these clumps are similar to the overall distribution of clump masses within the ATLASGAL survey. As the clumps hosting a maser are smaller than the full ATLASGAL clump sample, but have similar masses, the derived volume densities for maser associated clumps are significantly larger.

4.2 Stability and free-fall times

To test the stability of individual clumps, we can derive the virial parameter, which is defined as (Bertoldi & McKee 1992)

$$\alpha_{\mathrm{vir}} = \frac{5\sigma_v^2 R_{\mathrm{fwhm,pc}}}{G M_{\mathrm{fwhm}}}, \quad (2)$$

where σ_v^2 is the velocity dispersion of the NH_3 inversion transition emission observations (e.g. Urquhart et al. 2011; Wienen et al. 2012, 2018) and the other parameters are as previously defined. The virial parameter is a measure of the balance between gravitational collapse and internal energy that can counteract this collapse. A value of less than 2 generally indicates that an individual clump is unstable (Kauffmann et al. 2013) and is likely to be undergoing global gravitational collapse in the absence of any supporting magnetic fields.

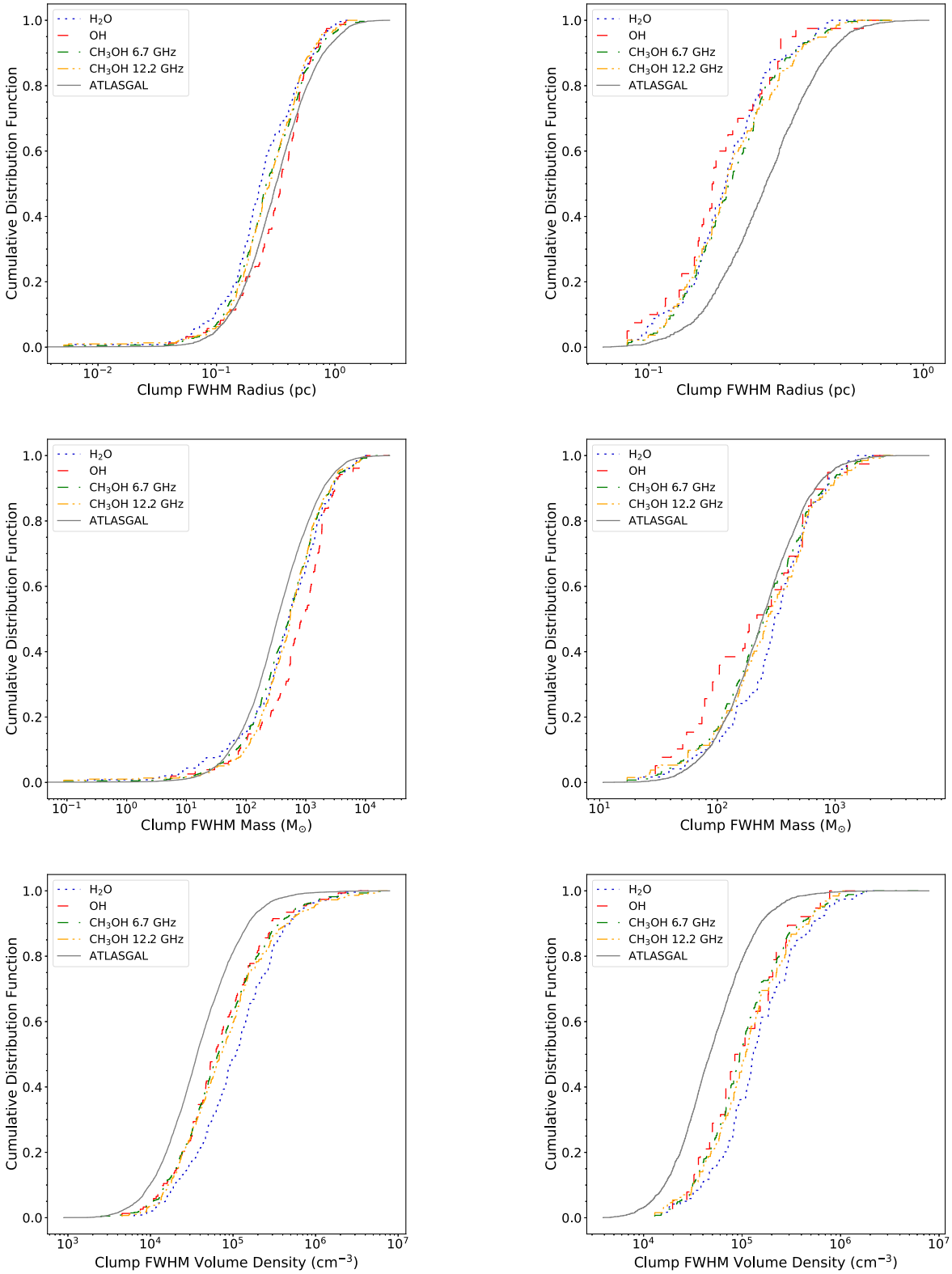

Figure 7. Clump FWHM radius, clump FWHM mass, and clump FWHM volume density distributions are presented in the upper, middle, and lower panels respectively. The cumulative distribution functions in the left-hand panels present the entire distributions of the maser associated clumps and the full ATLASGAL sample, whereas the cumulative distribution functions in the right-hand panels present a distance-limited sample (2–5 kpc) of the same distributions. Legends for each sample presented are shown in the top left-hand corner of each panel.

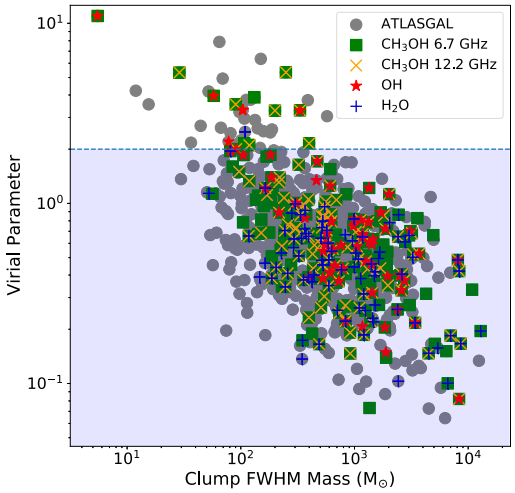

Figure 8. Virial parameters versus clump mass for maser associated clumps. This plot presents a distance-limited sample (2–5 kpc). The blue shaded area indicates the region of parameter space where clumps are gravitationally unstable (virial parameter < 2; Kauffmann, Pillai & Goldsmith 2013).

The virial parameter has been calculated for 741 ATLASGAL clumps (Urquhart et al. 2018). Fig. 8 presents the distribution of these virial parameters against clump FWHM mass for all clumps. We find that the majority of our clumps have a value lower than 2 and so are likely to be unstable to gravitational collapse, and no differing trends are seen between the maser samples.

Free-fall time-scales can be derived for each clump that have a corresponding FWHM volume density measurement

$$t_{\rm ff} = \sqrt{\frac{3\pi}{32G\rho}}, \tag{3}$$

where ρ is the mean volume density of a clump and G is the gravitational constant. The free-fall times for sources detected in ATLASGAL range between $\sim 2 \times 10^4$ and 2×10^6 yr. These free-fall times will be used to derive the statistical lifetime for each maser species in Section 5.2.2. When calculating the free-fall times of clumps, we have assumed that the dominant force is gravity and have not taken into account any support mechanisms that may impede the global collapse of clumps. However, given that ∼90 per cent of ATLASGAL clumps are associated with star formation it is safe to assume they are collapsing locally if not globally (Urquhart et al. 2018).

4.3 Maser and Bolometric luminosities

Maser luminosities have been calculated using the determined flux density values from the respective maser surveys and distance measurements taken from Urquhart et al. (2018). For consistency, we have used the peak maser fluxes rather than the integrated fluxes to determine the maser luminosities, as the Walsh et al. (2014) HOPS catalogue does not contain integrated fluxes as they focused on the distribution of individual maser spots. In Billington et al. (2019), we show that the differences between the peak and integrated fluxes for maser emission are insignificant above 1 Jy. The maser luminosities have units of Jy kpc^2 km s^{-1} and are, therefore, somewhat arbitrary. As in Billington et al. (2019), we have used conversion factors to convert the maser luminosities into solar units, a list of these factors can be found in Table 4 (see section 4.5 of Billington et al. 2019). The distribution of maser luminosities can be seen in Fig. 9. We find that the methanol and water masers have similar luminosities whereas

Table 4. Factors for converting the maser luminosities into units of L$_\odot$.

Maser transition frequency	Conversion factor (kHz)
22.235-GHz	74.1
1612-MHz	5.4
1665-MHz	5.6
1667-MHz	5.6
1720-MHz	5.7
6.7-GHz	22.3
12.2-GHz	40.7

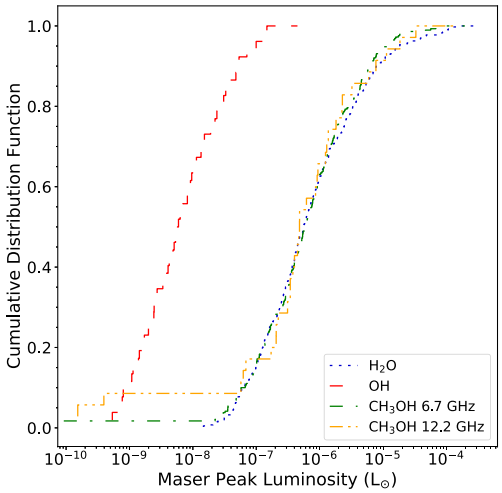

Figure 9. Cumulative distribution function showing a distance-limited samples (2–5 kpc) of the maser luminosities for all the species. The legend of each species is given the lower right-hand side of the plot.

the hydroxyl masers are significantly less luminous. Previous studies have also found similar results (e.g. Szymczak et al. 2005). This is expected as it has been theorized that OH masers are associated with the expanding material around H II regions. This material is less dense and so OH maser emission is weaker (Forster & Caswell 1989).

Bolometric luminosities have been taken unchanged from Urquhart et al. (2018). These luminosities have been calculated by reconstructing each sources' SED. A more detailed analysis of this method can be found in section 3 of König et al. (2017). Fig. 10 presents the distribution of luminosities as cumulative distribution functions (full sample and distance-limited sample). There appears to be no significant trends or differences between clumps associated with the different types of masers. Although they do appear to be significantly more luminous when compared to the full sample of clumps; this will be discussed in detail in Section 5.2.

4.4 Temperatures and $L_{\rm bol}/M_{\rm fwhm}$ ratios

Along with the physical parameters that have been derived in the previous subsections, we also define the $L_{\rm bol}/M_{\rm fwhm}$ ratio. This is the ratio between the bolometric luminosity of clumps and their corresponding FWHM mass, a distance independent quantity. Previous works have shown that this ratio is a good indicator of the evolutionary stage (Molinari et al. 2008, 2019), and so for the analysis within this study we shall use the $L_{\rm bol}/M_{\rm fwhm}$ ratios of clumps to determine the global evolutionary phase of these star formation regions. The $L_{\rm bol}/M_{\rm fwhm}$ ratios for the ATLASGAL sample range from $10^{-2.4}$ to $10^{3.3}$ L$_\odot$/M$_\odot$ with a mean of $10^{0.4}$ L$_\odot$/M$_\odot$. Fig. 11 presents the $L_{\rm bol}/M_{\rm fwhm}$ ratio

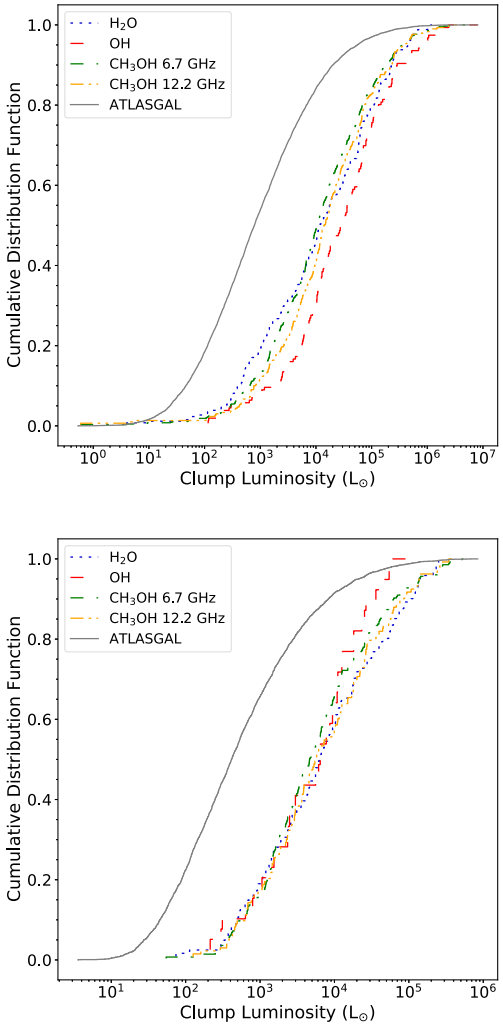

Figure 10. Clump luminosity parameter distributions. The cumulative distribution function in the upper panel presents the entire distribution of the maser associated clumps and the full ATLASGAL sample. The cumulative distribution function in the lower panel presents a distance-limited sample (2–5 kpc). Legends for each maser associated clump are given in the upper top left-hand side of both panels.

distributions as a cumulative distribution function, which will be further discussed in Section 5.2.1.

Temperatures for all clumps have also been utilized from the ATLASGAL survey (Urquhart et al. 2018). Along with the $L_{\rm bol}/M_{\rm fwhm}$ ratios, temperature is a good indicator of evolution as it has been shown that temperature and $L_{\rm bol}/M_{\rm fwhm}$ ratios of Galactic clumps are tightly correlated (see fig. 22 of Urquhart et al. 2018).

4.5 Uncertainties in physical parameters

The uncertainties in the distance measurements towards clumps are of the order of ±0.5 kpc and are estimated from the Bayesian distance algorithm presented in Reid et al. (2016). The uncertainty for radius is linearly correlated with the distance errors and this uncertainty is ∼30 per cent at 1 kpc but only a few percent at distances larger than 10 kpc. The mean error found when determining the dust temperature values from the SEDs is ∼10 per cent. The fractional uncertainty for the maser luminosities is roughly $\sqrt{2}$ times the fractional uncertainty in the distance measurements. However, in calculating this quantity

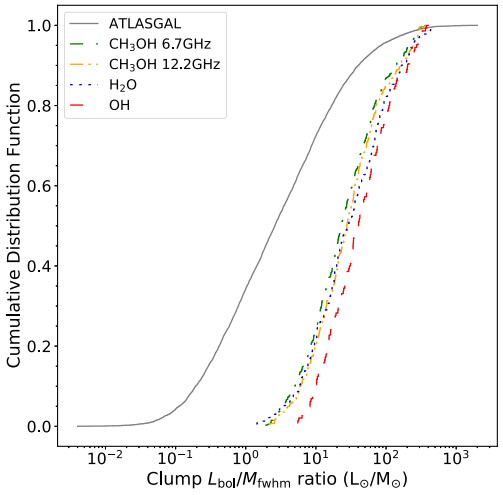

Figure 11. The cumulative distribution function of the $L_{\rm bol}/M_{\rm fwhm}$ ratios for all maser associated clumps. A legend is shown in the top left-hand side for each of the subsamples.

we are assuming the maser sources are emitting isotropically and so the uncertainty for these measurements are hard to estimate. As for the physical properties of the clumps, the error in the bolometric luminosities is a factor of a few due to the uncertainty on the bolometric flux values (15–50 per cent, depending on the wavelength of the observations; see König et al. 2017) and the distance errors. The uncertainty in the mass and volume density are likely dominated by the uncertainty in the value for the dust absorption coefficient (interpolated from Schuller et al. 2009 and taken to be 1.85 cm^2 g^{-1}) and the estimation of the dust-to-gas ratio (taken to be 100). Both of these parameters are poorly constrained and lead to uncertainties of a factor of ∼2–3. The uncertainties on the $L_{\rm bol}/M_{\rm fwhm}$ ratios are also a factor of a few, following the errors on the luminosity and mass calculations.

While the uncertainties in the physical parameters may be quite large, they affect the entire sample uniformly and will increase the scatter in the distributions. However, this will still allow for statistical trends to be identified and analysed, especially when considering a distance-limited sample. The use of a distance-limited sample will reduce biases of mass and size due to sensitivity limitations and the large range of distances to the clumps.

5 DISCUSSION

As in Billington et al. (2019), we have opted to only use the central 95 per cent (2σ) of parameter values within any given distribution. This will remove any potential errors or biases resulting from outliers due to inaccurate distance measurements or extreme sources.

5.1 Analysis tool: Kolmogorov–Smirnov test

Throughout this work, we employ the use of a two-sample Kolmogorov–Smirnov (KS) test. A two-sample KS test is a non-parametric test that compares the empirical cumulative distribution functions for two samples. The test measures the largest difference between two distributions and the associated confidence value, referred to as a p-value. The null hypothesis is that two samples are drawn from the same parent population. However, the null hypothesis can be rejected if the p-value is smaller than a selected confidence threshold (taken here as 3σ; i.e. $p < 0.0013$). This allows us to conclude that there is sufficient evidence to consider the samples

Table 5. The central 95 per cent of the L_{bol}/M_{fwhm} ratio, volume density (distance limited), and luminosities (distance limited) parameters for each maser species.

Maser species	L_{bol}/M_{fwhm} ratio ranges	Volume density ranges (cm^{-3})	Luminosity ranges ($L_\odot$)
Water	$10^{0.15}-10^{2.66}$	$10^{4.5}-10^{6.3}$	$10^{2.6}-10^{5.4}$
Hydroxyl	$10^{0.74}-10^{2.59}$	$10^{4.4}-10^{5.9}$	$10^{2.5}-10^{5.1}$
Methanol 12.2-GHz	$10^{0.32}-10^{2.60}$	$10^{4.2}-10^{6.0}$	$10^{2.6}-10^{5.4}$
Methanol 6.7-GHz	$10^{0.27}-10^{2.57}$	$10^{4.1}-10^{6.0}$	$10^{2.5}-10^{5.4}$

to be drawn from different populations and that two samples are significantly different from each other.

5.2 Physical parameters

Fig. 7 presents the full sample and distance-limited sample cumulative distribution functions of clump FWHM radius, FWHM mass, and FWHM volume density. It can be seen that the clumps associated with a maser are more compact than the full ATLASGAL sample, as presented in the upper right-hand panel of Fig. 7. The ratio between the mean clump radii for maser clumps versus non-maser clumps is 0.85. A two-sample KS test has also been applied to the radii of clumps associated with a maser source and the ATLASGAL sample to identify whether the difference in radii between the two samples is statistically significant. This has revealed that all of the maser associated clumps are significantly more compact than the rest of the dust clump sample ($p \ll 0.0013$).

We have also assessed the differences in temperature between clumps hosting a maser and those that do not. As can be seen in Table 3, clumps with associated maser emission are warmer than their non-maser counterparts. The mean temperature of a maser clump is 23.9 K whereas the mean temperature of an ATLASGAL clump is 19.4 K. We have also tested the samples using a KS test and find that the differences in temperature between the two samples is statistically significant ($p \ll 0.0013$). This difference has also been noted in another previous study by Jones et al. (2020), who examined a sample of 731 MMB sources with compact emission at four Hi-GAL wavelengths, and investigated the association between masers and Hi-GAL sources.

The masses of maser associated clumps are similar to the average mass of dense clumps and we do not find any significant differences, as confirmed by a KS test. As the clumps containing a maser are significantly more compact than the ATLASGAL sample, while having similar masses, the calculated volume densities are naturally increased. This shows that all maser species of interest are only associated with those clumps above a certain density threshold ($n(H_2) > 10^{4.1}$ cm^{-3}); this density limit is consistent with the result found in Billington et al. (2019) for the 6.7-GHz methanol masers.

Fig. 10 presents the distribution of clump luminosity for our various samples and we find that all of the maser clumps are more luminous by a factor of approximately 10 when compared to the average clump luminosity. The mean and median luminosities for maser associated clumps are both $\sim 10^4$ $L_\odot$. These values are ~ 2 times higher than those found by Jones et al. (2020), likely due to the differences in the way that the luminosity measurements were conducted. This implies that a certain protostellar luminosity is required, and therefore, protostellar mass in order to drive sufficient radiative and mechanical energy into the circumstellar environment to effectively pump the various maser species.

The physical parameters discussed above are all similar for each of the clumps associated with a different maser species, and all appear to be significantly larger when compared to the full ATLASGAL sample, except clump radius. These results do not completely conform with previous studies. For example, Breen & Ellingsen (2011) found that water masers are typically found towards clumps with larger radii, increased mass and increased luminosity. While we do find that masers are associated with clumps of increased luminosity, these clumps are found to be more compact than the larger ATLASGAL sample, and also have similar masses. This conflict is likely to be due to the source sample used in Breen et al. (2010), which originates from Hill et al. (2005). This millimetre study presented observations of 131 star-forming complexes suspected of harbouring massive star formation. The statistically significant differences between the samples presented in this study and Hill et al. (2005) can be attributed to the method of calculating the radii and masses of individual sources. The radii of millimetre sources in Hill et al. (2005) is highly dependent on the temperature of each region, an observational bias that is described in Billington et al. (2019), and instead we chose to calculated the sizes of sources based on the FWHM flux distribution. Moreover, Hill et al. (2005) used a constant temperature of 20 K to determine the mass of each clump, whereas the ATLASGAL temperatures are based on the results of SEDs, we therefore consider our results to be more reliable.

5.2.1 Evolutionary Stage – L_{bol}/M_{fwhm} ratios

Fig. 11 presents the cumulative distribution function for the L_{bol}/M_{fwhm} ratios of all the maser species and the full ATLASGAL sample. It can be seen from this Figure, that all the maser species occupy approximately the same distinct part of the parameter space, between $\sim 10^{0.2}$ and $10^{2.7}$ $L_\odot/M_\odot$. The exact ranges of the L_{bol}/M_{fwhm} ratios for each maser species can be found in Table 5.

We have tested the L_{bol}/M_{fwhm} ratios using clumps that have masses of >500 $M_\odot$ and by only using the clumps with the smallest offsets to their associated maser sources (spatial offset <10 arcsec, velocity offset <5 km s^{-1}). We find that these restrictions have no effect on the overall distributions of the L_{bol}/M_{fwhm} ratios for each maser sample, and the corresponding L_{bol}/M_{fwhm} ratio ranges. Since the L_{bol}/M_{fwhm} ratios of all of the maser associated clumps are similar (as confirmed by a KS test), this suggests that the mechanisms required for the production of any maser emission only occurs at a set stage in the evolution of star formation and then only for protostellar sources above a certain luminosity (~ 500 $L_\odot$).

In Fig. 12 we show clump FWHM volume density versus clump L_{bol}/M_{fwhm} ratio. It can be seen that there is a slight negative correlation between these two parameters. Although, this is likely to be due to the sensitivity limit of the ATLASGAL survey, which is also shown in the Figure. In Billington et al. (2019), a lower limit of volume density for 6.7-GHz methanol maser associated clumps was found to be $10^{4.1}$ cm^{-3}. This limit seems to hold for all of the maser species presented in this study, as shown in Fig. 12 and Table 5. Overall, our results show that certain physical conditions are necessary for the presence of any type of maser. These conditions are as follows: L_{bol}/M_{fwhm} of between $10^{0.2}$ and $10^{2.7}$, volume densities of above

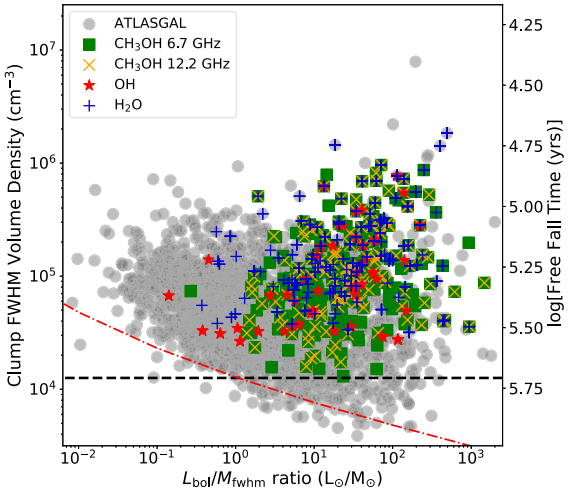

Figure 12. Distance-limited sample of volume density versus $L_{\rm bol}/M_{\rm fwhm}$ ratio for both the maser associated clumps and the full ATLASGAL sample. The entire ATLASGAL sample is shown in grey with the various maser species denoted by the legend in the upper left-hand corner of the plot. The sensitivity limits of the ATLASGAL survey is shown as the red dash-dotted line, determined for a distance of 2 kpc. The dotted black line at $y = 10^{4.1}$ cm^{-3} is the limit for 6.7-GHz maser emission to exist, as described in Billington et al. (2019).

$10^{4.1}$ cm^{-3}, and luminosities of above ∼500 L$_\odot$. This luminosity value corresponds to a protostellar mass of ∼6 M$_\odot$ assuming that $L \sim M^{3.5}$ (Kuiper 1938) and that the majority of a clump's luminosity arises from a single object. It also must be assumed that for this minimum mass to be accurate, any maser emission emanating from a clump must be associated with the most massive star. This scenario may not always be true, as it has been observed that water masers can arise from low-mass protostars. Naturally, these conditions are only required for masers present in star formation regions and may not hold true for the same maser species associated with other types of celestial objects.

5.2.2 *Statistical lifetimes*

Billington et al. (2019) presented the calculation of the statistical lifetime of the 6.7-GHz methanol maser by finding the ratio of maser associated clumps at specific volume density intervals and multiplying these by the free-fall times in these intervals. It was found that the mean statistical lifetime for this maser transition is ∼3.3 × 10^4 yr, which is in very good agreement with theoretical predictions (Van Der Walt 2005; 2.5−4.5 × 10^4 yr).

We have repeated this derivation for the maser species presented in this study. Free-fall times have been calculated for each clump within our sample that has a corresponding volume density measurement (as discussed in Section 4.2). These free fall times range from ∼20 000 to ∼750 000 yr. It is likely that any maser emission will only be present for a fraction of these time-scales and so by multiplying these times by the fraction of clumps associated with a particular kind of maser emission at specific volume density intervals, the statistical lifetime for maser emission can be found. Fig. 13 presents the clump ratios and statistical lifetimes for each maser species as a function of volume density. It can be seen from this Figure that the number of maser associated clumps increases with increased clump volume density. For the calculation of the statistical lifetimes, we only include clumps that have volume densities above our completeness limited for this

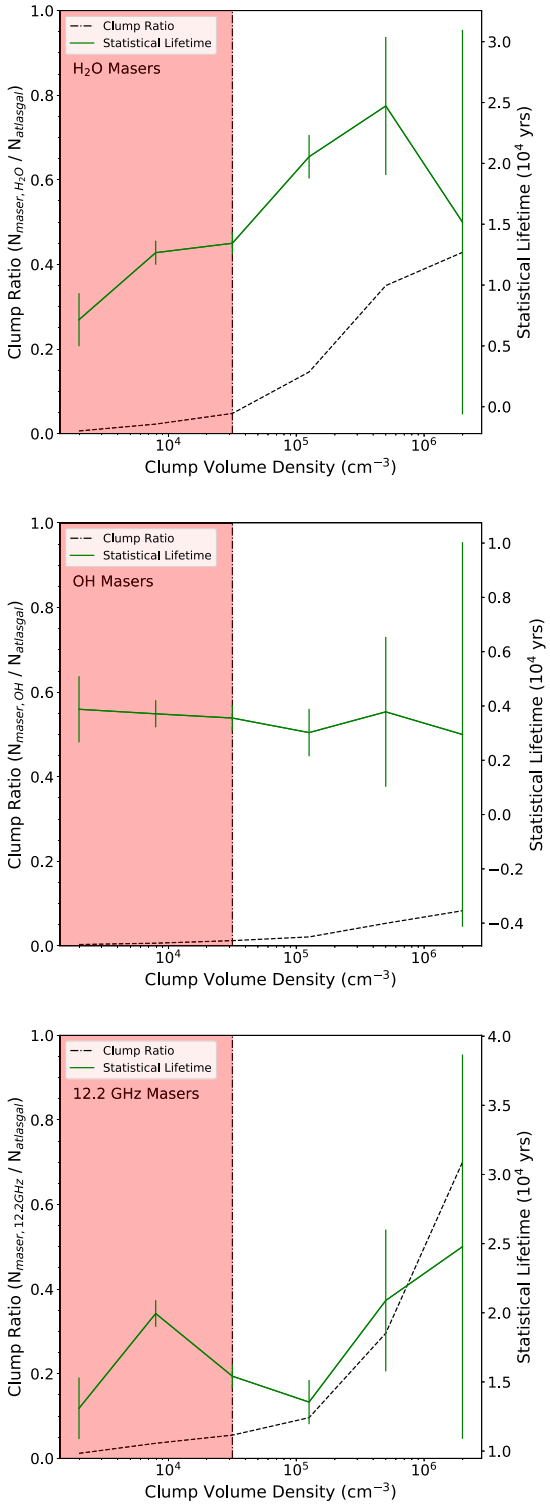

Figure 13. Plots presenting the clump ratios for each maser species and the statistical lifetimes as a function of clump FWHM volume density. The upper, middle, and lower panels present the lifetimes for the water, hydroxyl, and 12.2-GHz methanol masers, respectively. The black dotted lines shows the increasing number of maser associated clumps with respect to the volume density, whereas the solid green line presents the change in statistical lifetime for each volume density range. The shaded regions represents the parameter space where our sample is incomplete. Errors shown are derived from Poisson statistics.

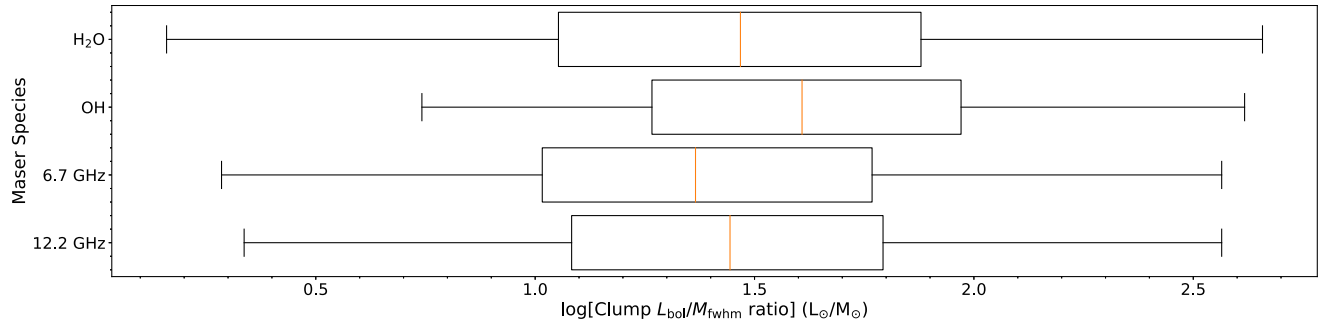

Figure 14. Box plot presenting the central 95 per cent distributions of $L_{\rm bol}/M_{\rm fwhm}$ ratios for clumps associated with the various maser species. Each box extends from the lower to upper quartile with an orange line denoting the median value, the whiskers show the full range of the data.

parameter, $n > 10^{4.5}$ cm^{-3} (Billington et al. 2019). We find that the mean lifetimes of maser emission to be 1.6, 0.4, and 2.0 $\times$ 10^4 yr for the water, hydroxyl and 12.2-GHz methanol masers respectively. The statistical lifetime for the 6.7-GHz maser is taken from Billington et al. (2019) as 3.3 $\times$ 10^4 yr. The uncertainty on these calculations has been calculated using Poisson statistics and is shown in Fig. 13, with the mean error being found to be $\sim$10 per cent. As the Poisson errors rely on the number of clumps at each volume density (error $= \sqrt{N}$, where N is the number of sources), the errors for the lifetimes are greatly increased towards higher volume densities due to the small number of clumps that possess these increase volume densities.

5.3 'Straw man' model comparison

One of the main aims of this study is to investigate the Ellingsen et al. (2007) 'straw man' model using the physical properties presented in the ATLASGAL catalogue. This model is based on maser observations within regions of ongoing star formation and that, methanol masers (class I and II) are associated with a very early stage of formation, followed by water masers. Hydroxyl masers are then seen to be coincident with ultracompact H II regions. In Section 5.2.1, we show that all of the maser associated clumps have similar $L_{\rm bol}/M_{\rm fwhm}$ ratios, which we are using as our gauge of protostellar evolution.

These differences between the $L_{\rm bol}/M_{\rm fwhm}$ ratios of the maser associated clumps can be used to investigate the 'straw man' model. In Fig. 14, we present a box plot of the distribution of $L_{\rm bol}/M_{\rm fwhm}$ ratios for the maser associated clumps. In general, there is a good agreement between the results presented in Fig. 14, and the previous model presented in Breen et al. (2010). However, a difference that can be noted is that water masers are seen towards regions of star formation before methanol masers and outlast hydroxyl masers, as predicted by the 'straw man' model. While these findings show that the 'straw man' model is fairly consistent with the $L_{\rm bol}/M_{\rm fwhm}$ ratios of associated clumps, it can be seen from Fig. 14 that there is a considerably overlap between all of the maser species, which limits the power of this model as an evolutionary tracer for star formation.

We can also attempt to test the 'straw man' model using the calculated statistical lifetimes for each maser phases. Breen et al. (2010) predicted that the lifetime of the 12.2-GHz methanol maser to be between 1.5 $\times$ 10^4 and 2.7 $\times$ 10^4 yr. The statistical lifetime that we calculate for this maser does lie towards the centre of this range at $\sim$2 $\times$ 10^4 yr, and so our results are in good agreement with Breen et al. (2010). Along with the statistical lifetime for the 6.7-GHz methanol maser predicted by Van Der Walt (2005) (2.5$-$4.5 $\times$ 10^4 yr) and the result found in Billington et al. (2019) ($\sim$3.3 $\times$ 10^4 yr) our results support the 'straw man' model in terms of the methanol masers. The model presented by Breen et al. (2010) predicts that the hydroxyl maser has a lifetime of $\sim$20 000 yr and the value found here is only a fifth of that prediction ($\sim$0.4 $\times$ 10^4 yr). Finally, water masers were predicted to have relative lifetimes of $\sim$30 000 yr, while we find a lifetime of approximately one half of this at only 16 000 yr. One aspect that has not been included in this study is the approximate lifetime of ultracompact H II (UCHIIs) regions, and where the maser lifetimes lie in comparison to this. The 'straw man' model predicts that UCHII regions begin to develop after the onset of water and 6.7-GHz methanol masers, and exist throughout the lifetime of the 12.2-GHz methanol masers and the hydroxyl masers. Kawamura & Masson (1998) predicted the dynamical age of a W3(OH) to be approximately 2 300 yr, similar to our prediction of the hydroxyl maser lifetime but an order of magnitude less than the 12.2-GHz statistical lifetime. Therefore, the 'straw man' model and our results may be overestimating the lifetime of the 12.2-GHz. However, it is currently unknown whether a UCHII region is required for the production of 12.2-GHz methanol masers and for how long after the development of a UCHII region could methanol maser emission be sustained.

All of the lifetimes that are estimated in this study are only a lower limit to the true lifetimes for each maser species, as the lifetimes depend on the sensitivity and completeness of each of the maser surveys. As these lifetimes are a lower limit on the true maser lifetimes, we find that they are still in agreement with the Ellingsen et al. (2007) model. While these measurements give a good indication of lifetimes for each maser species, we find it difficult to secure where these lifetimes lie in relation to one another as the $L_{\rm bol}/M_{\rm fwhm}$ ratios show no significant trends. Overall we find a good agreement with the 'straw man' model in terms of the statistical lifetimes of the maser species investigated, while having employed a different method to previous studies to calculate these lifetimes.

6 CONCLUSIONS

This study has investigated the correlations between the ATLASGAL catalogue and dense Galactic clumps that are associated with methanol, water and hydroxyl maser emission. We have used catalogues from the HOPS, THOR, SPLASH, MMB, and ATLASGAL surveys, along with 12.2-GHz MMB follow-up observations, to match maser emission to dense clumps located in the Galactic midplane ($|\ell| < 60^\circ$ and $|b| < 1.5^\circ$).

The association rates between maser emission and dust clumps for the 22.2-GHz water and 12.2-GHz methanol masers are found to be 56 and 82 per cent, respectively. The association rates for

the hydroxyl masers were found to be: 3 per cent (1612-MHz), 60 per cent (1665-MHz), 42 per cent (1667-MHz), and 49 per cent (1720-MHz). Physical parameters for the maser associated clumps and the full ATLASGAL sample are taken from Urquhart et al. (2018) and Billington et al. (2019).

(i) We find that the majority of methanol and water maser emission across the Galactic plane is associated with dense clumps, as identified by the ATLASGAL survey. Where a maser match has been found, they appear to have tightly correlated systematic velocities as those found for their counterpart clumps. The majority of masers (∼90 per cent) are also found to be tightly correlated with the peak of the dust emission (<10 arcsec), where the highest densities are found. This implies that they are at least coincident if not directly associated with embedded star formation.

(ii) It is just as common to find clumps coincident with multiple maser species (∼45 per cent) as those associated with only a single maser species (∼55 per cent). The communality of multiple species and/or transitions being found in a large fraction of clumps may be due to multiple evolutionary stages being present in each clump or that the various maser species require similar physical conditions. This is supported by the fact that all maser associated clumps, regardless of the corresponding maser species, have similar properties (we find no statistical differences between the clumps that are associated with different maser transitions).

(iii) Clumps associated with a maser are significantly more compact and dense than those that do not host any maser emission. However, we find no differences in radius and volume density between clumps which are associated with different maser species.

(iv) There is a similar density threshold required for the production of all species of maser emission as found in Billington et al. (2019) (clump densities of greater than $10^{4.1}$ cm^{-3}), further justifying that volume density is an important factor for maser emission. Furthermore, the fraction of clumps with associated maser emission increases with volume density.

(v) The $L_{\rm bol}/M_{\rm fwhm}$ ratios of maser associated clumps, regardless of the associated maser emission, are shown to occupy the same distinct region of the parameter space, and so all types of maser emission can be seen to have similar turn-on and turn-off points in the evolutionary sequence. The 'straw man' model (Ellingsen et al. 2007) predicts that the different maser species turn on and off at different times, however, large uncertainties associated with our results have limited any detailed comparison with the model but the $L_{\rm bol}/M_{\rm fwhm}$ ratios are broadly consistent with previous findings.

(vi) We have constrained the physical properties required for maser emission and it is shown that masers only exist in clumps with volume densities above $10^{4.1}$ cm^{-3}, luminosities greater than ∼500 L$_\odot$ and also require a minimum protostellar mass, estimated to be ∼6 M$_\odot$. Maser species also have an approximate turn-on point in the evolutionary process of star formation (∼$10^{0.2}$ L$_\odot$/M$_\odot$).

(vii) Statistical lifetimes are calculated for the water, hydroxyl and 12.2-GHz methanol masers, and these lifetimes are found to be ∼1.6, 0.4, and 2.0 × 10^4 yr, respectively. We find that the lifetimes for the 6.7-GHz (as found in Billington et al. 2019) and 12.2-GHz methanol masers are in good agreement with the values predicted by Breen et al. (2010), whereas the statistical lifetimes determined for the water and hydroxyl masers are considerably shorter than those predicted, by one quarter and one half, respectively. The lifetimes calculated for all masers are a lower limit on the true lifetimes, and so, our results support the 'straw man' model (Ellingsen et al. 2007).

ACKNOWLEDGEMENTS

S J B wishes to acknowledge an STFC (Science and Technology Facilities Council) PhD studentship for this work. H B acknowledges support from the European Research Council under the Horizon 2020 Framework Program via the ERC Consolidator Grant CSF-648505, and RSK via the ERC Advanced-Grant 339177 (STARLIGHT). HB further acknowledges support from the Deutsche Forschungsgemeinschaft in the Collaborative Research Center (SFB 881) 'The Milky Way 74 System' (subproject B1). We have used the collaborative tool Overleaf available at: https://www.overleaf.com/.

DATA AVAILABILITY

The data underlying this paper will be shared on a reasonable request to the corresponding author.

REFERENCES

Argon A. L., Reid M. J., Menten K. M., 2000, ApJS, 129, 159
Batrla W., Matthews H. E., Menten K. M., Walmsley C. M., 1987, Nature, 326, 49
Bertoldi F., McKee C. F., 1992, ApJ, 395, 140
Beuther H., Walsh A., Schilke P., Sridharan T. K., Menten K. M., Wyrowski F., 2002, A&A, 390, 289
Beuther H. et al., 2016, A&A, 595, A32
Beuther H. et al., 2019, A&A, 628, A90
Bihr S. et al., 2016, A&A, 588, A97
Billington S. J. et al., 2019, MNRAS, 2798, 2779
Błaszkiewicz L., Kus A. J., 2004, A&A, 413, 233
Breen S. L., Ellingsen S. P., 2011, MNRAS, 416, 178
Breen S. L., Ellingsen S. P., Caswell J. L., Lewis B. E., 2010, MNRAS, 401, 2219
Breen S. L., Ellingsen S. P., Caswell J. L., Green J. A., Voronkov M. A., Avison A., Fuller G. A., Quinn L. J., 2012a, MNRAS, 421, 1703
Breen S. L., Ellingsen S. P., Caswell J. L., Green J. A., Voronkov M. A., Fuller G. A., Quinn L. J., Avison A., 2012b, MNRAS, 426, 2189
Breen S. L., Ellingsen S. P., Contreras Y., Green J. A., Caswell J. L., Stevens J. B., Dawson J. R., Voronkov M. A., 2013, MNRAS, 435, 524
Breen S. L. et al., 2014, MNRAS, 438, 3368
Breen S. L. et al., 2015, MNRAS, 450, 4109
Breen S. L., Ellingsen S. P., Caswell J. L., Green J. A., Voronkov M. A., Avison A., Fuller G. A., Quinn L. J., 2016, MNRAS, 459, 4066
Breen S. L. et al., 2018, MNRAS, 474, 3898
Caswell J. L., 2004, MNRAS, 349, 99
Caswell J. L., Vaile R. A., Ellingsen S. P., Norris R. P., 1995, MNRAS, 274, 1126
Caswell J. L. et al., 2010, MNRAS, 404, 1029
Caswell J. L. et al., 2011, MNRAS, 417, 1964
Caswell J. L., Green J. A., Phillips C. J., 2013, MNRAS, 431, 1180
Cheung A. C., Rank D. M., Townes C. H., Thornton D. D., Welch W. J., 1969, Nature, 221, 626
Churchwell E. et al., 2009, PASP, 121, 213
Claussen M. J., Wilking B. A., Benson P. J., Wootten A., Myers P. C., Terebey S., 1996, ApJS, 106, 111
Claussen M. J., Goss W. M., Frail D. A., Desai K., 1999, ApJ, 522, 349
Codella C., Lorenzani A., Gallego A. T., Cesaroni R., Moscadelli L., 2004, A&A, 417, 615
Contreras Y. et al., 2013, A&A, 549, A45
Cragg D. M., Sobolev A. M., Ellingsen S. P., Caswell J. L., Godfrey P. D., Salii S. V., Dodson R. G., 2001, MNRAS, 323, 939
Cragg D. M., Sobolev A. M., Godfrey P. D., 2002, MNRAS, 331, 521
Csengeri T. et al., 2014, A&A, 565, A75
Dawson J. R. et al., 2014, MNRAS, 439, 1596
Eden D. J. et al., 2017, MNRAS, 469, 2163
Elitzur M., 1992, ARA, 30, 75

Elitzur M., Goldreich P., Scoville N., 1976, ApJ, 205, 384
Elitzur M., Hollenbach D. J., Mckee C. F., 1989, ApJ, 346, 983
Ellingsen S. P., Voronkov M. A., Cragg D. M., Sobolev A. M., 2007, Proc. Int. Astron. Union, 242, 213
Forster J. R., Caswell J. L., 1989, A&A, 213, 339
Goedhart S., Gaylard M. J., Van Der Walt D. J., 2005, Astrophys. Space Sci., 295, 197
Green J. A. et al., 2009, MNRAS, 392, 783
Green J. A. et al., 2010, MNRAS, 409, 913
Green J. A. et al., 2012, MNRAS, 420, 3108
Guzmán A. E., Garay G., Brooks K. J., Voronkov M. A., 2012, ApJ, 753, 51
Henning T., Lapinov A., Schreyer K., Stecklum B., Zinchenko I., 2000, A&A, 364, 613
Hill T., Burton M. G., Minier V., Thompson M. A., Walsh A. J., Hunt-Cunningham M., Garay G., 2005, MNRAS, 363, 405
Jones B. M. et al., 2020, MNRAS, 493, 2015
Kauffmann J., Pillai T., Goldsmith P. F., 2013, ApJ, 779, 185
Kawamura J. H., Masson C. R., 1998, ApJ, 509, 270
König C. et al., 2017, A&A, 599, 1
Kuiper G. P., 1938, ApJ, 88, 472
Menten K. M., 1991, ApJ, 380, L75
Menten K. M., 1997, Proc. IAU Symp. 178, International Astronomical Union, Molecules in Astrophysics: Probes and Processes. Kluwer, Dordrecht, p. 163
Menten K. M., Reid M. J., Pratap P., Moran J. M., Wilson T. L., 1992, ApJ, 401, L39
Minier V., 2000, A&A, 362, 1093
Minier V., Ellingsen S. P., Norris R. P., Booth R. S., 2003, A&A, 403, 1095
Molinari S., Pezzuto S., Cesaroni R., Brand J., Faustini F., Testi L., 2008, A&A, 481, 345
Molinari S. et al., 2010, PASP, 122, 314
Molinari S. et al., 2019, MNRAS, 486, 4508
Moore T. J. et al., 2015, MNRAS, 453, 4264
Motte F., Schilke P., Lis D. C., 2002, in Crowther P. A., ed., ASP Conf. Ser. Vol. 267, Massive Star Formation in the Galactic Mini-Starburst W43. Astron. Soc. Pac., San Francisco, p. 393
Norris R. P. et al., 1998, ApJ, 508, 275
Phillips C. J., Norris R. P., Ellingsen S. P., McCulloch P. M., 1998, MNRAS, 300, 1131
Qiao H., Li J., Shen Z., Chen X., Zheng X., 2014, MNRAS, 441, 3137
Qiao H.-H. et al., 2016, ApJS, 227, 26
Qiao H.-H. et al., 2018, ApJS, 239, 15
Reid M. J., Dame T. M., Menten K. M., Brunthaler A., 2016, ApJ, 823, 1
Rosolowsky E. et al., 2010, ApJS, 188, 123
Schuller F. et al., 2009, A&A, 504, 415
Siringo G. et al., 2009, A&A, 497, 945
Sobolev A. M., Cragg D. M., Godfrey P. D., 1997, A&A, 324, 211
Szymczak M., Kus A. J., Hrynek G., Kepa A., Pazderski E., 2002, A&A, 392, 277
Szymczak M., Pillai T., Menten K. M., 2005, A&A, 434, 613
Thomasson P., 1986, QJRS Astron. Soc., 27, 413
Titmarsh A. M., Ellingsen S. P., Breen S. L., Caswell J. L., Voronkov M. A., 2014, MNRAS, 443, 2923
Titmarsh A. M., Ellingsen S. P., Breen S. L., Caswell J. L., Voronkov M. A., 2016, MNRAS, 459, 157
Urquhart J. S. et al., 2011, MNRAS, 418, 1689
Urquhart J. S. et al., 2013, MNRAS, 431, 1752
Urquhart J. S. et al., 2014a, MNRAS, 443, 1555
Urquhart J. S. et al., 2014b, A&A, 568, A41
Urquhart J. S. et al., 2015, MNRAS, 446, 3461
Urquhart J. S. et al., 2018, MNRAS, 473, 1059
Van Der Walt J., 2005, MNRAS, 360, 153
Walsh A. J., Burton M. G., Hyland A. R., Robinson G., 1998, MNRAS, 301, 640
Walsh A. J. et al., 2011, MNRAS, 416, 1764
Walsh A. J., Purcell C. R., Longmore S. N., Breen S. L., Green J. A., Harvey-Smith L., Jordan C. H., Macpherson C., 2014, MNRAS, 442, 2240
Walsh A. J. et al., 2016, MNRAS, 455, 3494
Wang Y. et al., 2018, A&A, 619, A124
Weinreb S., Barrett A. H., Meeks M. L., Henry J. C., 1963, Nature, 200, 829
Wienen M., Wyrowski F., Schuller F., Menten K. M., Walmsley C. M., Bronfman L., Motte F., 2012, A&A, 544, A146
Wienen M., Wyrowski F., Menten K. M., Urquhart J. S., Walmsley C. M., Csengeri T., Koribalski B. S., Schuller F., 2018, A&A, 609, A125
Wilson W. J., Barrett A. H., 1968, ApJS, 73, 209
Xu Y., Li J. J., Haschisuka K., Pandian J. D., Menten K. M., Henkel C., 2008, A&A, 485, 729
Yang K. et al., 2017, ApJ, 846, 160
Yang K. et al., 2019, ApJS, 241, 18

This paper has been typeset from a TEX/LATEX file prepared by the author.